

Spin Transfer Efficiency

Karl Ahrendsen

February 19, 2020

Chapter 1

Report

1.1 Introduction

Over the past 6 months, I have been collecting data with the Rubidium (Rb) Spin Filter Apparatus to better understand the effect of buffer gases on the ability to extract a beam of spin polarized electrons from a polarized Rb gas and incident beam of unpolarized electrons. This represents the latest efforts in the continued development of this apparatus.

My specific goal with this dataset was to determine the best buffer gas species, pressure, and Rb number density combination to maximize the extracted electron polarization. For a given buffer gas type and pressure, three spin transfer efficiency datasets were collected at differing n_{Rb} , spanning 1.5 orders of magnitude. The target densities were 3×10^{12} , 10×10^{12} , and $30 \times 10^{12} \frac{\text{atoms}}{\text{cm}^3}$.

The idea to collect this dataset was developed in collaboration with Dr. Tupa. The logic behind the necessity for this dataset is as follows. When n_{Rb} is low the Rb polarization will be high- nearly 100%, as one does not have to combat with the effects of radiation trapping at these densities. Despite the high P_{Rb} , the P_e will not be at its maximum value because there aren't enough Rb atoms for the free electrons to spin-exchange with and obtain a polarization. In the opposite direction, with a high n_{Rb} there will be enough Rb atoms for the free electrons to interact with, but P_{Rb} will be lower due to the effects of radiation trapping. Therefore, there must be some intermediate n_{Rb} for which P_{Rb} remains high, but there are enough Rb atoms that the free electrons are able to interact and obtain their polarization. This idea was summarized in a series of notes Dr. Tupa and I recorded to communicate the concept. These notes have been photocopied and are available at the end of the report in the Appendix (Chapter 2).

Dr. Tupa had initially suggested collecting the data at whatever maximum buffer gas pressure we could obtain. This original idea was abandoned when the viewports quickly became coated with an opaque substance. The substance appears when running the system with either N₂ or ethene, though the effects

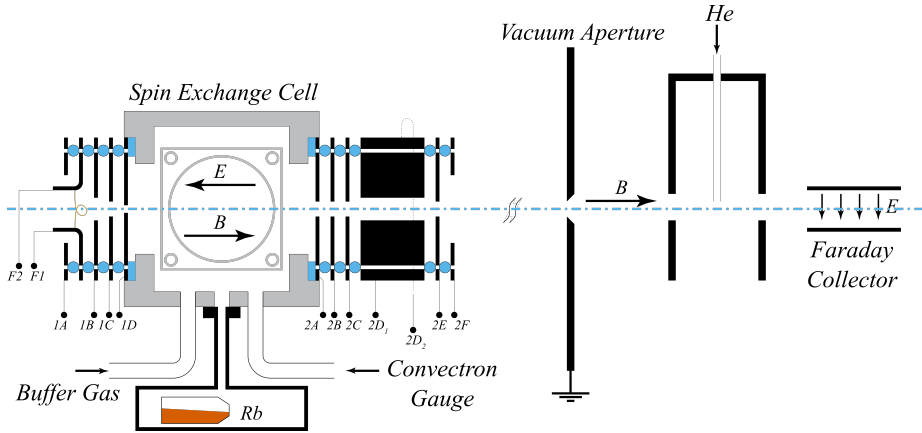


Figure 1.1: A schematic of the electron gun with the names of the electrodes for referencing the potentials.

did seem to be more pronounced when operating the system with ethene.

1.2 Methods

1.2.1 Data Collection

For all but one experiment contained in this report, the incident electron energy was held constant at 100 eV. I consciously chose to keep the electrodes at the same potential throughout the run, though I may have failed in this respect with one electrode's potential. The wiring used was Munir's, save for the entrance and exit electrodes which referenced the target instead of ground. A diagram of the system can be found in Fig. 1.1, and the potentials that optimize electron transmission as well as Munir's typical potentials are shown in Table 1.1

Two difference specie of buffer gas were used in this study, N_2 and C_2H_4 . Since Convecron gauges assume Nitrogen in their pressure readouts, a correction must be made to the readout of the gauge to get the true pressure in the system when ethene is being used. Grandville Phillips' instruction manual for the gauge has calibration curves for a number of gases, but it does not include ethene. We used the calibration curve for methane (CH_4) instead. Our experiments were conducted in a range of buffer gas pressures (1-1,000 mTorr) where a simple offset is used to correct the convecron gauge. For the values reported here, I have assumed a gauge reading of

$$600 \text{ mTorr } C_2H_4 = 375 \text{ mTorr } N_2 \quad (1.1)$$

That is, the gauge readings for ethene were multiplied by .625 to obtained the true pressure in the system. This correction has been applied to the ethene pressures reported in this document.

| Electrode Name | 100eV Value | Pirbhai's 100eV | 2eV Value | Pirbhai's 2eV |
|----------------|-------------|-----------------|-----------|---------------|
| 1A | -152.2 | -141 | -44.3 | -37 |
| Filament | -140.5 | -141 | -37 | -37 |
| 1B | -120 | -112.5 | 23.5 | -8.5 |
| 1C | -127 | -100 | 16.1 | 4.1 |
| 1D | -43.2 | -35 | -35 | -35 |
| Collision Cell | -40.2 | -33 | -34 | -33 |
| 2A | -37.1 | -30 | -31 | -30 |
| 2B | 0 | 10 | -39.3 | 10 |
| 2C | -18.7 | N/A | -18.6 | N/A |
| 2D1 | -10 | 0 | -.4 | 0 |
| 2D2 | -10 | 9 | .4 | 9 |
| 2E | 0 | 0 | 0 | 0 |
| 2F | 0 | 0 | 0 | 0 |

Table 1.1: Potentials the electrodes were set to for this run and comparisons to the values that I assume Pirbhai used. I am simply translating the potentials that he notes in his thesis and converting them to reference ground, assuming that he made no adjustments to the tuning and simply increased the “Filament” value to obtain different incident energies.

The general procedure for collecting data at a given n_{Rb} and BGP is as follows.

1. Set the BGP leak valve to a value which corresponds to the desired BGP.
2. Set the filament current to 4.5 A.
3. Set the variacs so that the reservoir achieves the desired temperature and the collision cell is roughly 20°C hotter than the reservoir. The number densities probed required reservoir variac settings between 18 and 26 V.
4. Configure the system to collect absorption scans, doing so every 10 minutes.
5. Monitor the absorption scans to track how much Rb is in the system.
6. When the density is roughly $1 \times 10^{12} \frac{\text{atoms}}{\text{cm}^3}$, configure the system to collect Faraday rotation data.
7. Continue monitoring the density through the Faraday rotation data until it has reached an equilibrium point.
8. If the equilibrium point is a quarter order of magnitude different from a data point that has already been collected, proceed to collecting a spin transfer dataset. If not, adjust the variac setting and again wait for an equilibrium value.

9. If time permits, collect data for another n_{Rb} value. Adjust the variac and monitor the density through Faraday rotation and repeat the above steps.

Collecting a Spin Transfer Dataset

Collecting a Spin Transfer Dataset consists of a background measurement and a signal measurement. For most datasets, I collected the background data before the signal, but in some instances the order was reversed.

The background measurement was typically preceded by an “energy defining excitation function” where I would determine the potential at which I should set the helium target to be at the peak of the excitation function. Once that was determined, I could collect background data for the polarimeter at that Helium target potential.

Collecting the background data consisted of 26 polarization runs divided into:

Beam off background Of the 26 runs 9 were collected with the beam off.

The 9 runs are divided equally into three categories, pump laser off, pump laser pumping with σ_+ light and pump laser pumping with σ_- light.

A “Beam off” run means that the electron beam is prepared as normal except the deflector plates are set to the maximum voltage, steering the electron beam away from the Faraday collector. No electron current should be reaching the detector, though operationally, there was a 7 nA signal on the ammeter. The number of counts did not increase though, indicating that this was not truly an electron beam.

Gas off background Of the 26 background runs, 15 runs were collected without helium gas in the polarimeter chamber. These 15 runs are divided equally into three categories, in the same way as the “Beam off” background.

A “Gas off” run means that the electron beam is prepared as normal except the helium gas is turned off.

Collecting the signal for the spin transfer dataset was automated by a computer script. The script would first collect electron polarization data, then measure the Rubidium polarization, then collect excitation function/ retarding field analysis (RFA). Once this had been completed, the pump laser frequency would be adjusted and the whole process was repeated. The pump laser frequency was changed in 2 GHz steps, starting at 3 GHz and ending at 11 GHz. The peak polarization is typically obtained at 2.75 GHz.

The electron polarization data consisted of 15 full revolutions of the polarimeter divided equally into 3 categories. The three categories are pump laser blocked, σ_+ light, and σ_- light- collected in that order. The categories were interleaved, so the first and fourth runs were both pump laser blocked runs.

After the electron polarization the Rb polarization was measured with Faraday rotation. This was accomplished with 3 “Faraday scans” where the plane

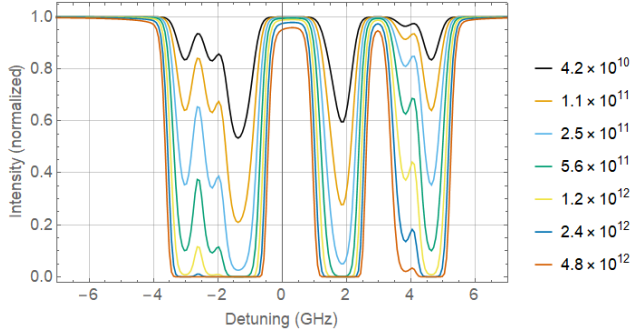


Figure 1.2: Expected absorption profiles at densities below $5 \times 10^{12} \frac{\text{atoms}}{\text{cm}^3}$. These are used to get a rough estimate of the number density in the system while the chamber is warming.

of linear polarization of the probe laser is measured at 6 detunings. These scans were divided into the same categories as mentioned for the polarization data.

After the Faraday scans, two excitation functions are collected. One is collected with the pump laser blocked and one with the pump laser on.

1.2.2 Data Analysis

Absorption Scan

Absorption scans are collected regularly to monitor the density of Rb present in the system. Absorption scans are used primarily when the amount of Rb less than $1 \times 10^{12} \frac{\text{atoms}}{\text{cm}^3}$, once the density is above this threshold, the Faraday rotation method provides a much more precise way to calculate the density. Using the absorption scans, I can measure a density as low as $4.2 \times 10^{10} \frac{\text{atoms}}{\text{cm}^3}$.

These were used to give an indication to the progress of warming the Rubidium as the system was first starting up. A more rigorous method could be used to obtain a number density for a given scan, but I chose to qualitatively compare the scans to simulated data for a rough estimate. To this end, I compared the scans obtained to a series of profiles, shown in Fig. 1.2 and Fig. 1.3.

Excitation Function

Excitation functions are analyzed in a similar manner to Absorption scans. Often, simply observing the plotted data is all the required analysis. The key feature which is sought is where the helium fluorescence begins. The location of the beginning is not made with an algorithm- it was simply my discretion. Once the energy where the counts began rapidly increasing was identified, I added 7 eV to this energy and set the Helium potential to this value when collecting polarization data.

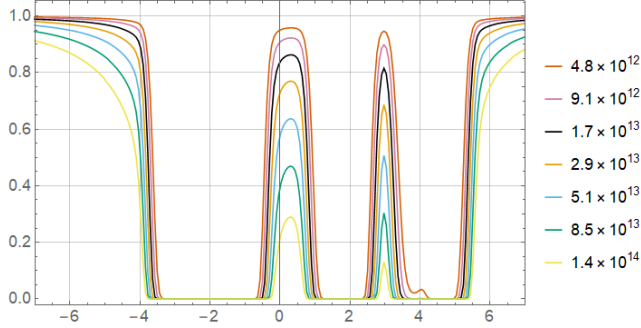


Figure 1.3: Expected absorption profiles at densities above $4 \times 10^{12} \frac{\text{atoms}}{\text{cm}^3}$. These are used to get a rough estimate of the number density in the system while the chamber is warming.

Faraday Rotation n_{Rb}

The equation that I use to calculate n_{Rb} is given by

$$n_{Rb} = \frac{2h}{r_e c \mu_B} \frac{\nu_o^2}{f_{ge} \kappa} \frac{A_2}{\int B \cdot dL} \quad (1.2)$$

Where the variables have the following meanings, and the units are chosen such that the number density will be reported in particles per cubic centimeter. The exact values which I used can be found in the appendix.

- A_2 = fitting parameter, see below
- h = Planck's constant
- ν_o = line center frequency
- L = the length of the cell
- r_e = classical radius of the electron
- c = speed of light in a vacuum
- f_{ge} = transition strength
- κ = constant arising from selection rules [3, pg. 95]
- B = magnetic field strength
- μ_B = Bohr Magneton
- n_{Rb} = rubidium number density
- $\Delta\theta$ = Faraday rotation angle
- ν = frequency of probe laser

The fitting parameter A_2 comes from fitting the following equation to the collected data.

$$\bar{\theta}(\nu) = \frac{A_2 \nu_o^2 \nu^2}{c^2 (\nu - \nu_o)^2} + \frac{A_4 \nu_o^2 \nu^2}{c^4 (\nu - \nu_o)^4} \quad (1.3)$$

I analyzed the number density using 4 data points at probe laser detunings of -30, -15, 15, and 30 GHz from the Rb line center. The equation fitting is done using Mathematica and I am confident in my implementation as I have analyzed some of Munir's Faraday rotation data with my program and arrived at the same answer that Munir calculated.

Faraday Rotation P_{Rb}

The formula that I use to calculate the polarization is

$$P_{Rb} = C \frac{a}{Ln_{Rb}} \quad (1.4)$$

Where the variables have the following meanings, and the units are chosen such that the polarization is reported as a decimal number with 1 being 100 percent.

a = a fitting parameter, see below

C = collection of polarization constants, see below

L = the length of the cell (cm)

n_{Rb} = rubidium number density (particles/cm³)

The fitting parameter a is the slope of the fit to the linear relationship between the inverse of the probe detuning $\delta_{pr.}$ and the Faraday rotation angle $\Delta\theta$.

$$\Delta\theta = \frac{P_{Rb}Ln_{Rb}}{C} \frac{1}{\delta_{pr.}} \quad (1.5)$$

$\delta_{pr.}$ = Detuning of the probe laser (GHz)

$\Delta\theta = \theta - \theta_B$ (rad.)

θ = pr. laser angle of linear polarization while pumping (rad.)

θ_B = pr. laser angle of linear polarization B field applied (rad.)

We let

$$a = P_{Rb} \frac{Ln_{Rb}}{C} \quad (1.6)$$

and solve for P_{Rb} to find Eq. 1.4

The constant C is a collection of constants that will not change during the course of the experiment. It is

$$C = \frac{4 \times 10^9 \text{ Hz}}{r_e c} \frac{1}{f_{ge}} = 1.38323 \times 10^{12} \text{ cm}^{-3}$$

To calculate my polarization, I collect data at four different probe laser detunings, -30, -15, 15, and 30 GHz from the Rb line center. I have analyzed some of Pirbhai's data with my code and our calculations agree to around 6%.

Electron Polarization

I calculate my electron polarization using a Helium optical polarimeter. Electrons excite Helium atoms causing light to be emitted, the polarization of which is related to the incident electron polarization. The electron polarization is calculated from the stokes components of the light through the relation

$$P_e = P_3 \left(\frac{2.6409}{1.0614 + 0.9386 P_1} \right) \quad (1.7)$$

as determined by Pirbhai [4].

Electron Polarization Analysis

The process of measuring the electron polarization is similar to collecting Faraday Rotation data because we must also rotate an optical element and collect the intensity of light at a number of positions. The intensity data is first background subtracted, then the Fourier coefficients of the light intensity versus optical element angular position are calculated.

These coefficients, in combination with the initial positions of the pass axis of the optical elements, are used to determine the polarization of the Helium fluorescence. Based on the polarization of the Helium fluorescence, we can then calculate the polarization of the electrons.

The process of obtaining an electron polarization measurement is outlined here, but is a replication of the analysis performed by Berry et. al [1]:

1. First collect data recording intensity and QWP position from N equally spaced positions of the QWP. N should be no less than 16 to ensure oscillations at all necessary frequencies are available. (Collect Data)
2. Normalize the data. At a minimum, the count rate should be divided by the current on the Faraday cup. Another component of normalizing might be removing background. The resultant value is then called the signal. (Normalize Polarization Data)
3. Fourier Analyze the signal to obtain the coefficients of the C_0, C_2, S_2, C_4, S_4 functions. (Fourier Analyze Data)
4. Use these Fourier coefficients with the initial position of the linear polarizer and quarter-wave plate to calculate the stokes parameters of the Helium fluorescence (Calculate Stokes From Fourier Data)
5. Use the stokes parameters of the light to calculate the electron polarization. (Calculate Electron Polarization from Stokes)

I collect data at 16 different positions on the stepper motor. I previously collected data with 60 data points, and developed these figures at that time. The raw data looks something like Fig. 1.4.

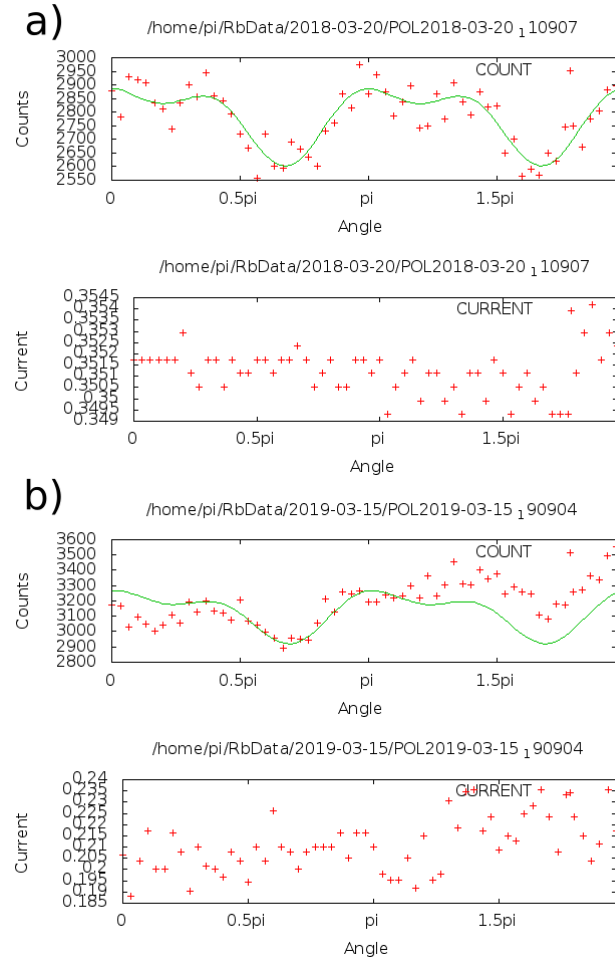


Figure 1.4: Displayed here are two sets of data, one that is exceptionally low noise (a), the second is a more typical set of data (b). In both sets of data, the fit is to the current-normalized intensity, while the displayed data points have not been normalized to the current. The variation on the recorded current is an order of magnitude higher in (b), resulting in the apparently poor fit.

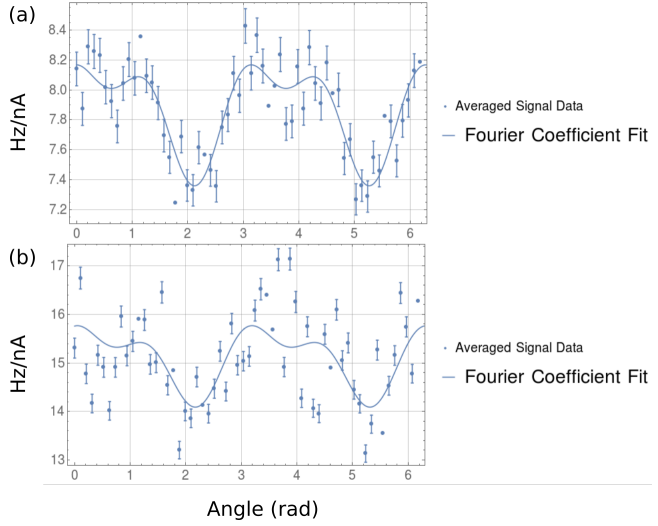


Figure 1.5: Item (a) is the “clean” data and item (b) is the “typical” data.

We then normalize the current and subtract away the dark counts. See Section 1.2.2 for details on this process. After normalizing the counts to the current and subtracting the dark counts, the intensity should be somewhere in the range of 5 to 20 Hz/nA. The data hasn’t changed much, but it looks like Fig. 1.5.

We then Fourier analyze the data with a discrete Fourier transform, obtaining Fourier coefficients for all frequencies up to $N/2$. We can get a rough idea of how noisy the data is by simply comparing the relative magnitudes of the Fourier components. We expect the Fourier coefficients at frequencies of 2 and 4 to have the largest values. A visualization of the values of the Fourier components is shown in Fig. 1.6.

With the Fourier coefficients, we calculate the Stokes parameters of the light. These formulas are included here, reproduced from Berry (with the correction of a typo):

$$\begin{aligned}
 P_0 &= C_o - \frac{1 + \cos(\delta)}{1 - \cos(\delta)} [C_4 \cos(4\alpha + 4\beta_o) + S_4 \sin(4\alpha + 4\beta_o)] \\
 P_1 &= \frac{2}{1 - \cos(\delta)} [C_4 \cos(2\alpha + 4\beta_o) + S_4 \sin(2\alpha + 4\beta_o)] / P_0, \\
 P_2 &= \frac{2}{1 - \cos(\delta)} [S_4 \cos(2\alpha + 4\beta_o) + C_4 \sin(2\alpha + 4\beta_o)] / P_0, \\
 P_3 &= \frac{C_2}{\sin(\delta) \sin(2\alpha + 2\beta_o)} / P_0 = \frac{S_2}{\sin(\delta) \cos(2\alpha + 2\beta_o)} / P_0, \\
 |P_3| &= \frac{(C_2^2 + S_2^2)^{1/2}}{\sin^2(\delta)} / P_0
 \end{aligned} \tag{1.8}$$

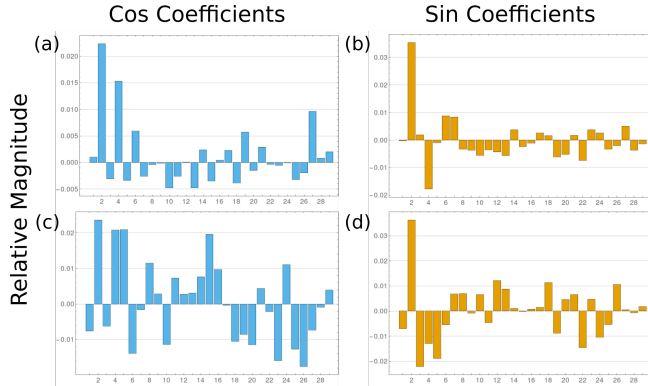


Figure 1.6: Images (a) and (b) and the coefficients for the “clean” data and images (c) and (d) are the coefficients for the “normal” data. Note that the magnitude of the coefficients other than 2 and 4 relative to 2 and 4 are much higher in c) and d). This is an indication of the noise in the data, according to Berry.

For our two sets of data, the stokes parameters are shown in Fig. 1.7.

With the stokes parameters of the light, we can then determine the polarization of the electrons using the equation that Munir cites in his thesis.

$$P_e = P_3 \left(\frac{2.6409}{1.0614 + 0.9386 P_1} \right) \quad (1.9)$$

Carrying through the calculation, we find that each of these runs has an 8% polarization.

To determine an error associated with this value, I collect multiple polarization runs, calculate the electron polarization for each run, and report the mean as the electron polarization for the run. The standard deviation of the mean is used as the error in the measurement.

Electron Polarization Background Subtraction

The process of subtracting background from the polarimeter follows that developed by Clayburn as written in his thesis [2]. I found some aspects of the discussion and notation confusing, so I will reproduce it in my own words here.

A background measurement consists of a “beam off” background run and a “gas off” background run. The “beam off” run measures the background that comes from sources that are not related to the electron beam. The “gas off” run measures background that comes from the electron beam, but is not part of the helium fluorescence. The beam off intensity could also be thought of as “dark counts” so I note these counts with the symbol D .

| Clean | | Typical | |
|--------|------------|---------|-----------|
| p0 | 7.76025 | p0 | 14.8123 |
| p1 | 0.0439101 | p1 | 0.0451495 |
| p2 | -0.0036779 | p2 | 0.0099495 |
| p3_mag | 0.0427074 | p3_mag | 0.0443357 |
| p3_c2 | 0.724962 | p3_c2 | 0.767083 |
| p3_s2 | 0.0359892 | p3_s2 | 0.0370694 |

Figure 1.7: The stokes parameters for the two sets of data previously displayed. Note that with the exception of P_0 the values are very similar.

$$D_\beta = \sum_{i=1}^{n_D} \frac{D_{\beta i}}{n_D t} \quad (1.10)$$

and it's error which is

$$\delta D_\beta = \pm \left(\sum_{i=1}^{n_D} \frac{D_{\beta i}}{n_D^2 t^2} \right)^{\frac{1}{2}} \quad (1.11)$$

Where

n_D = number of dark count measurements

t = time over which each measurement was collected

β = angular position of the polarimeter reatarder

These dark counts will be present in any data we collect, so they will be subtracted from the next intensity that we measure from the “gas off” or electron beam dependent counts. Since the dark counts are not dependent on current, we should subtract the dark counts from the beam dependent counts before we normalize with current.

We give the beam dependent intensity the symbol B and we write this symbolically as

$$B_\beta = \sum_{i=1}^{n_B} \left(\frac{B_{\beta i}/t - D_\beta}{n_B I_\beta} \right) \quad (1.12)$$

$$\delta B_\beta = \pm \left(\sum_{i=1}^{n_B} \frac{B_{\beta i}/t^2 - (\delta D_\beta)^2}{n_B^2 I_\beta^2} \right)^{\frac{1}{2}} \quad (1.13)$$

Here n_B is used in the same sense as in Eq. 1.10, and the variable I_β represents the magnitude of the current collected on the Faraday cup at the time of the count measurement. We now have in B the intensity of the background.

Now for removing the background from the measurement M . Again, we first subtract the dark count rate from the raw measurement count rate. We then normalize with respect to the current. After this normalization, the background intensity can be subtracted from the measurement. I then have S the background removed signal which we can analyze to determine the polarization of the light.

$$S_{\beta i} = \left(\frac{M_{\beta i}/t - D_\beta}{I_\beta} - B_{\beta i} \right) \quad (1.14)$$

$$\delta S_{\beta i} = \pm \left(\frac{M_{\beta i}/t^2 - (\delta D_\beta)^2}{I_\beta^2} - (\delta B_\beta)^2 \right)^{\frac{1}{2}} \quad (1.15)$$

Note that I do not average the signal counts at this point. Instead, I calculate the electron polarization for each run, and

1.3 Results

Here are the linear fits of all of the data:

1.3.1 200 mTorr

The data collected at 200 mTorr is shown in Fig. 1.8.

1.3.2 400 mTorr

The data collected at 400 mTorr is shown in Fig. 1.9.

1.3.3 800 mTorr

The data collected at 800 mTorr is shown in Fig. 1.10 for N_2 . There is no corresponding data for C_2H_4 as the viewport became blocked to quickly to collect any data.

1.3.4 Munir Recreation ($E_i=2$ eV, 200 mTorr N_2)

One difference between the majority of the spin transfer data I have collected here and the data that Munir collected is the incident energy of the electrons, E_i . I typically collect data at $E_i=100$ eV because much higher currents can be achieved with the higher incident electron energy. I decided to collect additional data at the lower incident energy to verify that this difference isn't the cause of our low efficiency values. Fig. 1.11 shows the results.

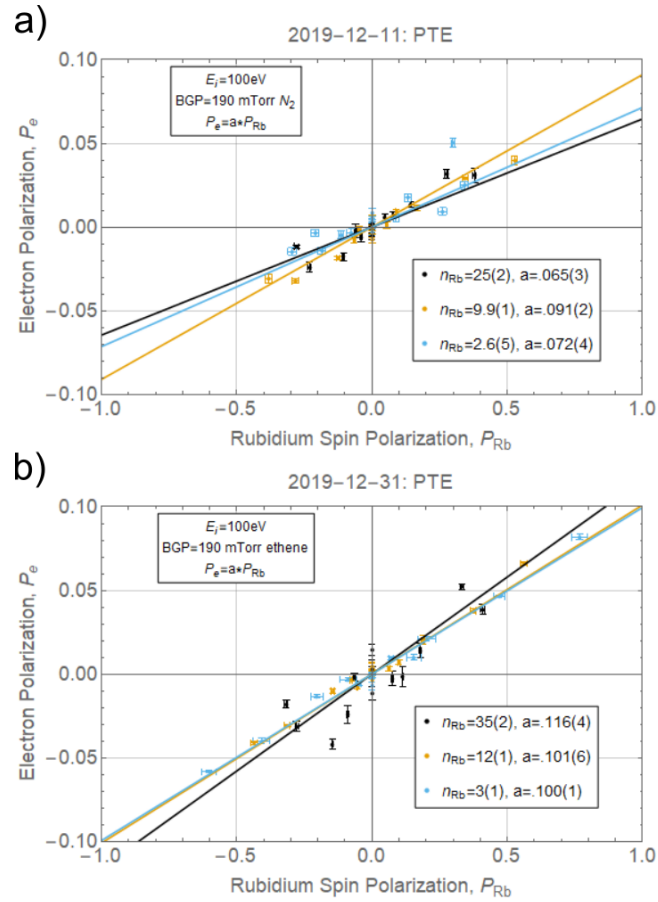


Figure 1.8: The spin transfer efficiency data for at 200 mTorr. The top graph labeled a) shows the N_2 data while the bottom graph b) shows the C_2H_4 data.

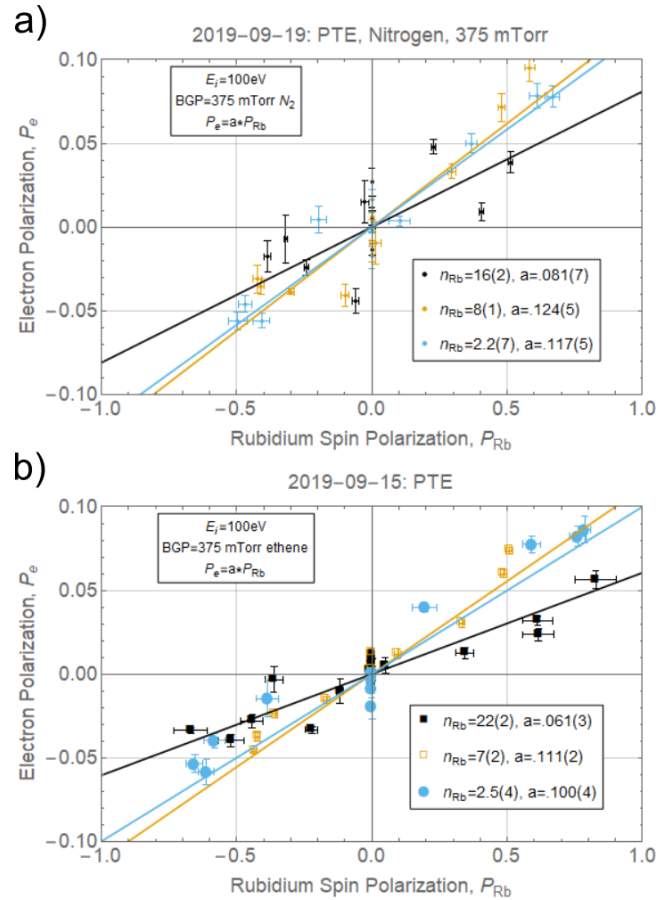


Figure 1.9: The spin transfer efficiency data for at 400 mTorr. The top graph labeled a) shows the N_2 data while the bottom graph b) shows the C_2H_4 data.

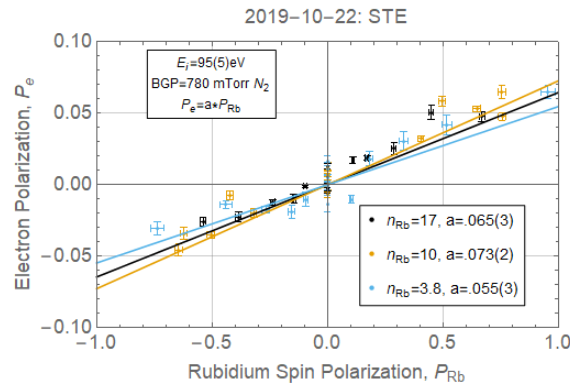


Figure 1.10: The spin transfer efficiency data for N_2 at 800 mTorr.

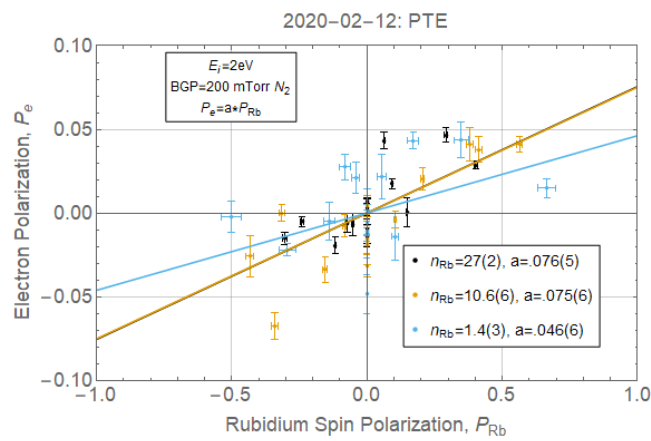


Figure 1.11: Spin transfer efficiency data collected with an incident electron energy of 2 eV. The buffer gas pressure was 200 mTorr for these measurements.

| bgt | bgp | low | mid | high | lowd | midd | highd |
|----------------|-----|-------|-------|-------|------|------|-------|
| ethene | 200 | 0.1 | 0.101 | 0.116 | 3 | 12 | 35 |
| nitrogen | 200 | 0.072 | 0.091 | 0.065 | 2.6 | 10 | 25 |
| ethene | 375 | 0.1 | 0.111 | 0.061 | 2 | 7 | 23 |
| nitrogen | 375 | 0.117 | 0.124 | 0.081 | 2.2 | 8 | 16 |
| nitrogen | 780 | 0.059 | 0.066 | 0.065 | 3.8 | 10 | 17 |
| nitrogen (2eV) | 200 | 0.046 | 0.075 | 0.076 | 1.4 | 10.6 | 27 |

Table 1.2: The calculated slopes for each of the spin transfer efficiencies presented in this document. The buffer gas type (bgt), and buffer gas pressure (bgp) in mTorr are listed first. Because obtaining the exact same density with our system is difficult, the data were not collected at the exactly the same buffer gas pressures from run to run. I group them according to the closest target density (low= 3×10^{12} , mid= 10×10^{12} , high= 30×10^{12}). The measured densities in each run are then listed in units of $1 \times 10^{12} \frac{\text{atoms}}{\text{cm}^3}$.

1.3.5 Tabular Data

The calculated slopes for the datasets each of the datasets are presented in tabular form in Table 1.2.

1.4 Discussion

The spin transfer efficiency data lacks a clear indication on the effect of either buffer gas pressure or n_{Rb} on spin transfer efficiency. A statistical difference between the slopes is present, but the underlying data is sufficiently noisy to call into question the validity and utility of that difference. The clearest conclusion is that an intermediate number density appears to maximize the spin transfer efficiency. This is what we anticipated when we began collecting data, but we expected a different reason for this optimal density.

Unfortunately, a lower E_i was not the panacea to our low polarization issues. The spin transfer efficiencies are low and the data collected at $E_i=2$ eV has more noise than the $E_i=100$ eV data.

While collecting the $E_i=2$ eV data, I also observed an unexpected dependence of transmitted current on pump laser detuning. I recorded more current on the Faraday cup when the pump laser was tuned to the D1 line of Rb. This increase in current was a function of the Rb density in the system. The corresponding data is shown in Fig. 1.12.

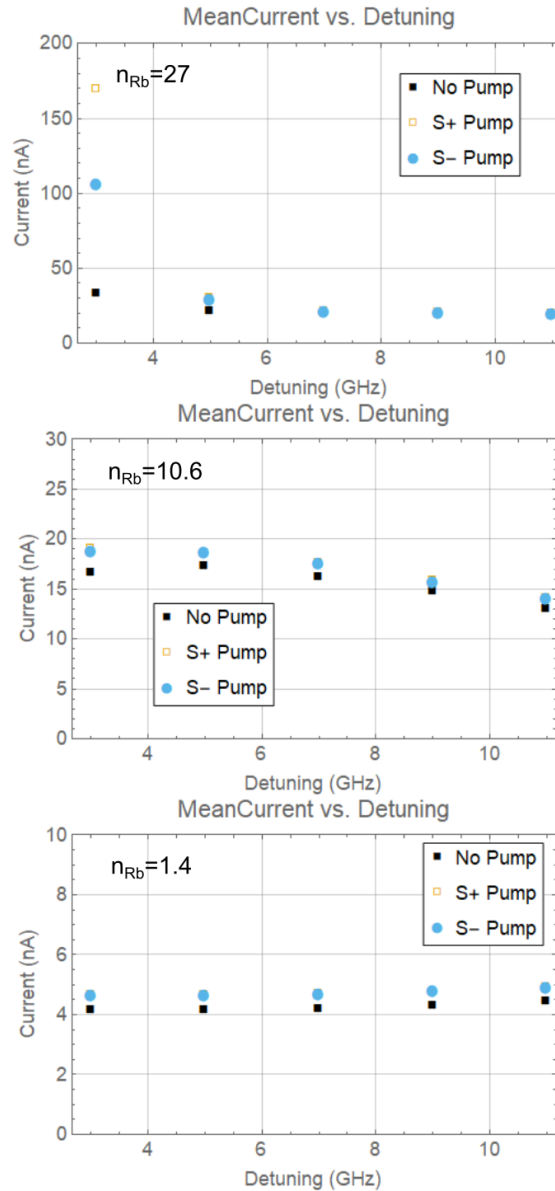
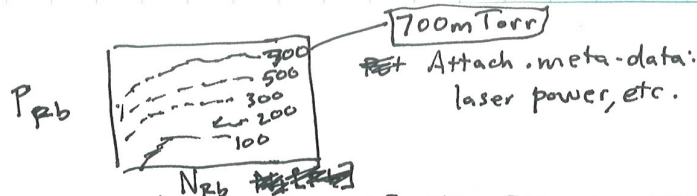


Figure 1.12: Average current measured on the polarization run. There is a dependence on both the pump laser detuning and n_{Rb} . The effect is most pronounced at $n_{Rb}=27 \times 10^{12}$, but a small effect can be seen when $n_{Rb}=10.6 \times 10^{12}$. The effect appears to be completely absent when $n_{Rb}=1.4 \times 10^{12}$

Chapter 2

Appendix

2.1 Dale's Notes

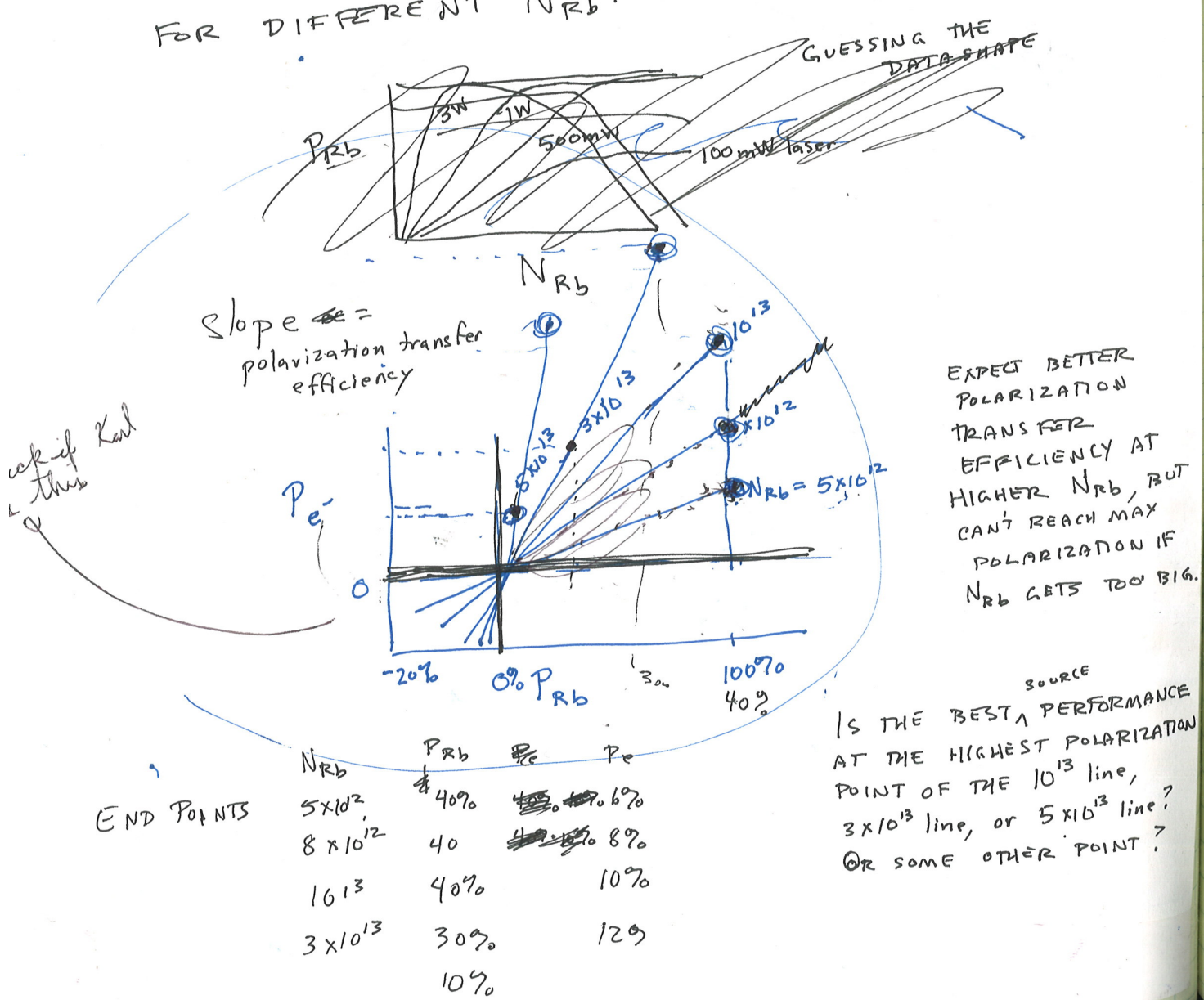


2019-06-29
DALE TUPA
MEETING NOTES

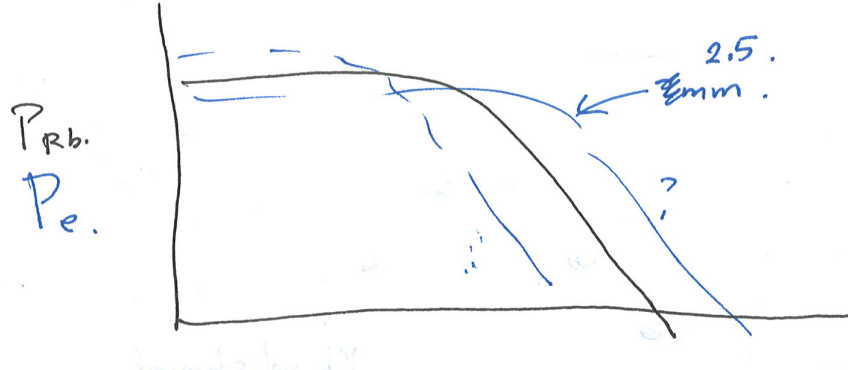
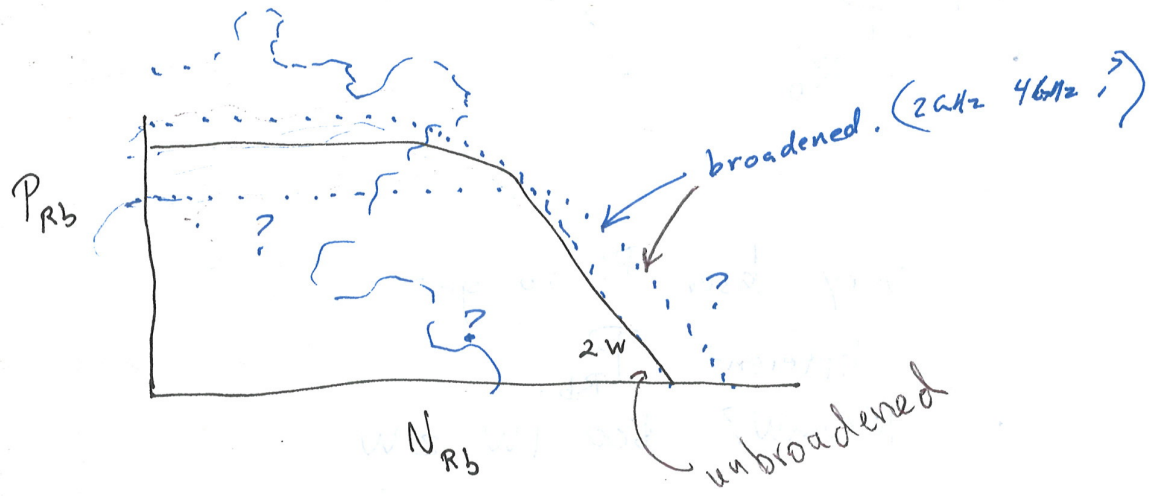
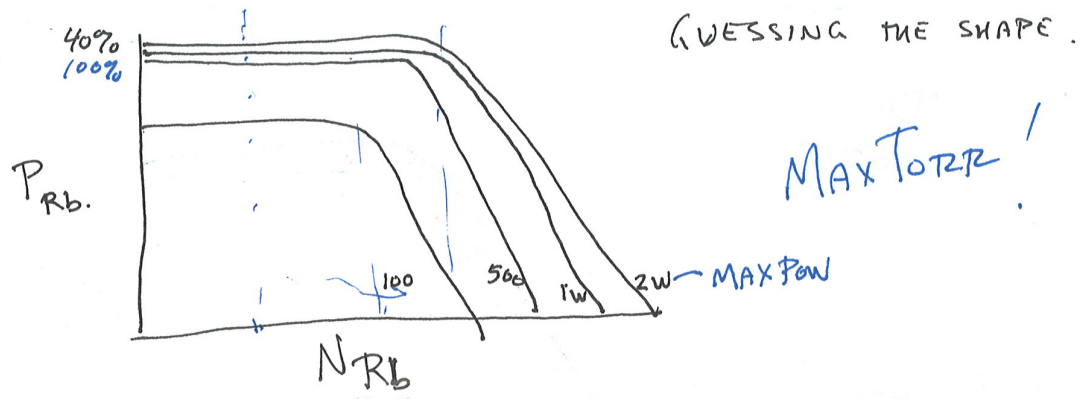
1. * UNTIL THERE'S EVIDENCE TO DO OTHERWISE, PERFORM ALL EXPTS AT 500mTorr.*

* Look up pump specs. See if this can be renamed 700mTorr or even higher.

2. TAKE DATA TO UNDERSTAND P_{Rb} vs. ~~N_{Rb}~~ AND P_e vs. N_{Rb} . BE CAREFUL SO THAT THE SAME DATA CAN BE USED TO SHOW THE EFFICIENCY OF POLARIZATION TRANSFER BETWEEN Rb AND e^- FOR DIFFERENT N_{Rb} .



2A

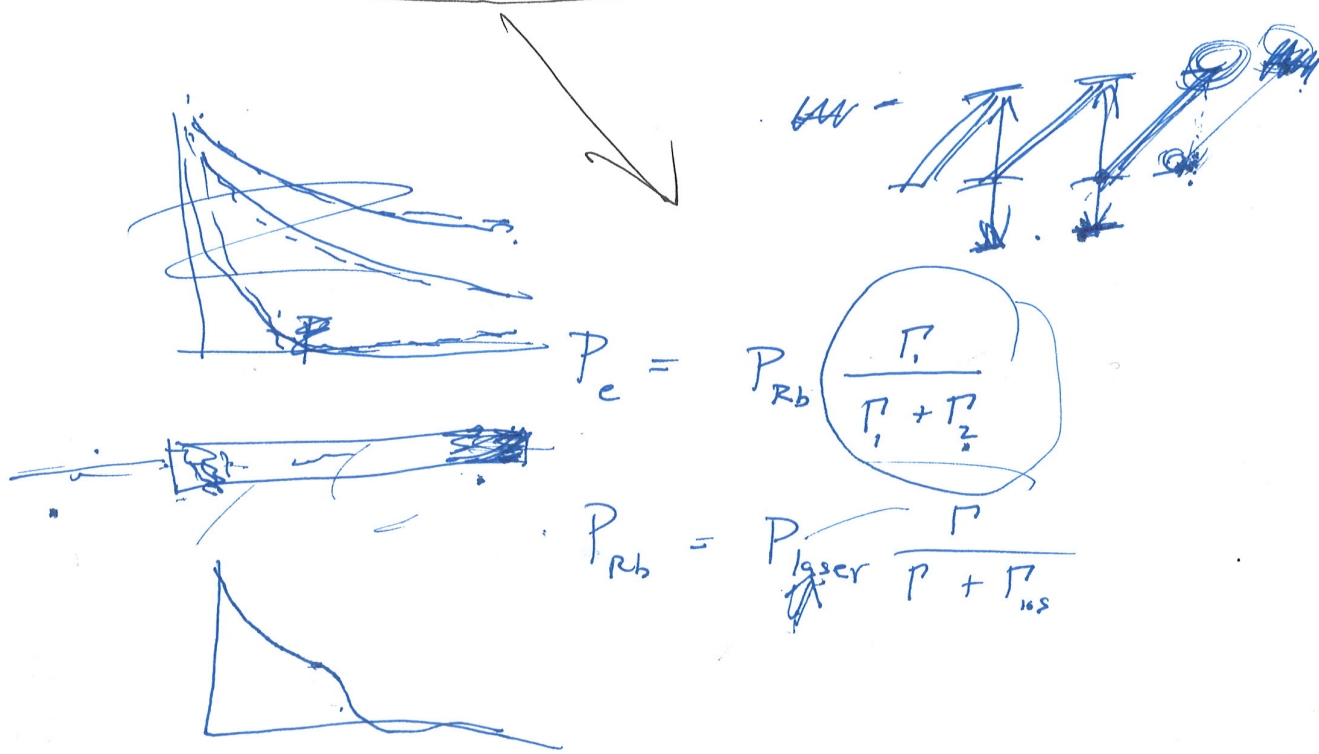


Look up filament behavior.

3) DOES TRANSFER EFFICIENCY IMPROVE
(OR GET WORSE, OR NO CHANGE?)
IF ATOMS ARE MORE OFTEN IN
EXCITED STATE?

PUT PUMP
LASER ON
CYCLING
TRANSITION.
THIS ONLY WORKS
IF YOU ALSO
HAVE A
REPUMP
LASER.

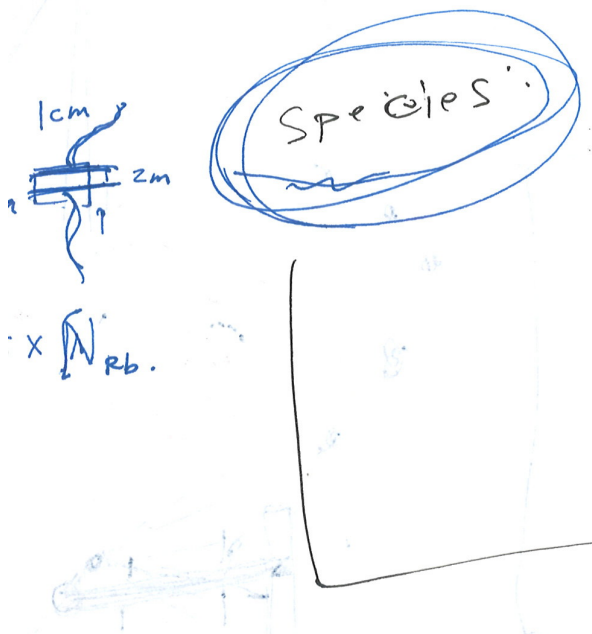
4) DOES TRANSFER EFFICIENCY
IMPROVE WITH 2 mm DIAMETER
AND/OR
ULTIMATE Rb POLARIZATION
PUMP BEAM?



COLLISIONAL
ELECTION TRANSPORT.



$\beta \beta P_{\text{Buffer.}}$



Species

$\times N_{Rb.}$

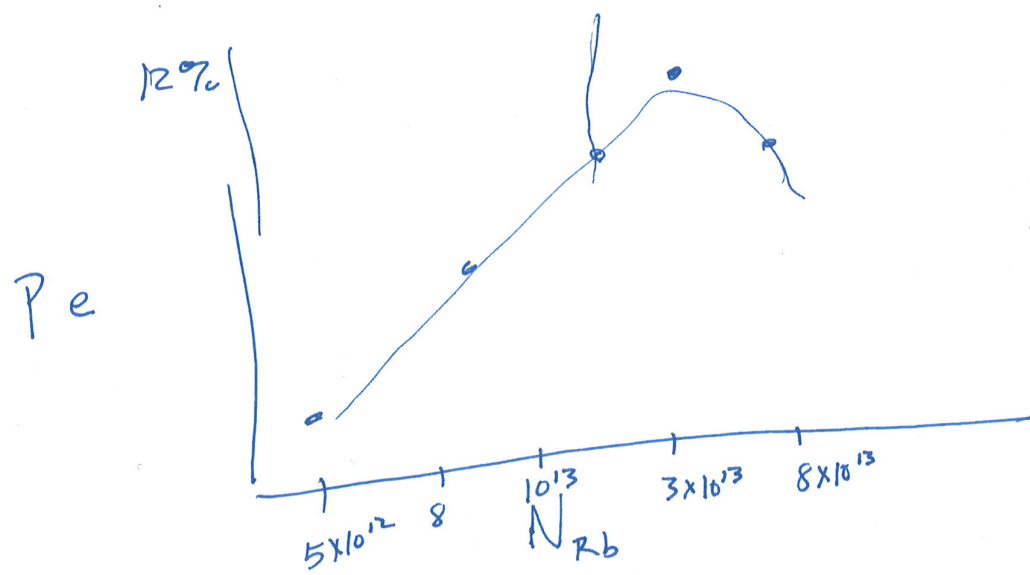
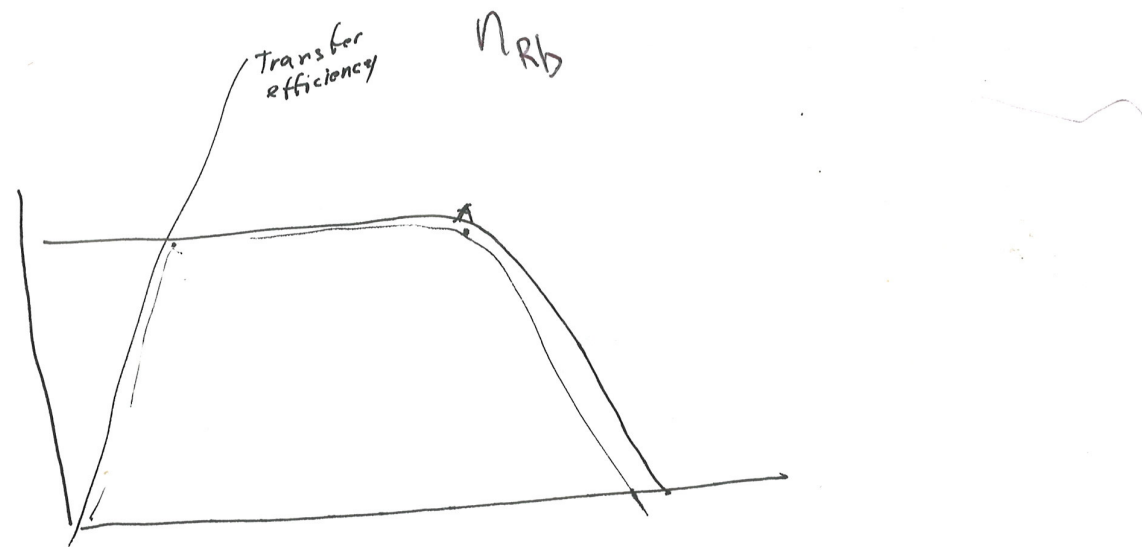
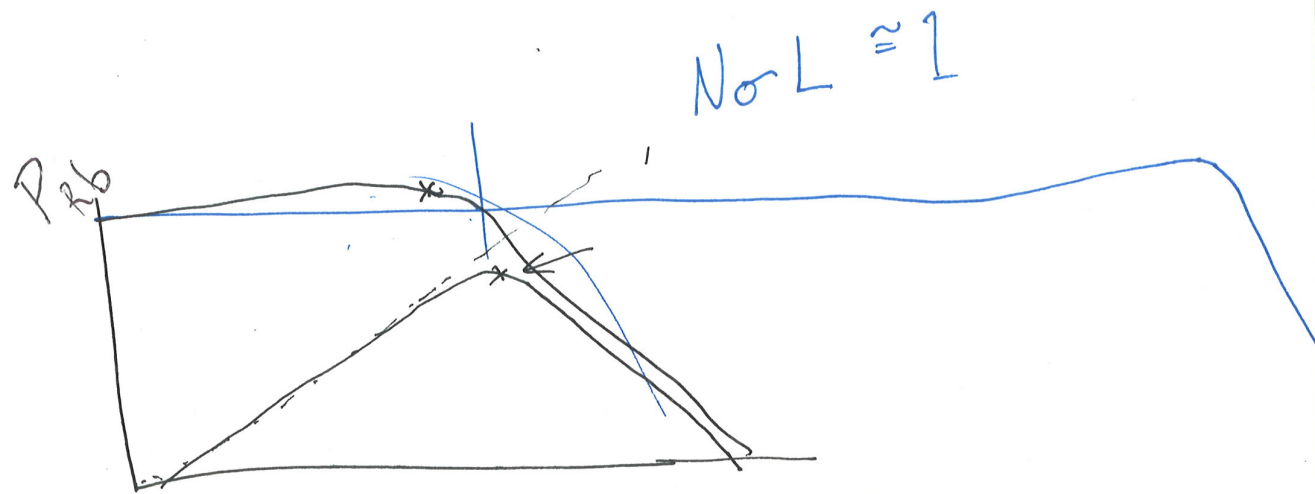
N_2 Ethylen

~~k_{fc}~~

$x+1$

actir

in



2.2 Constants

Here is a list of the physical constants that I used and their numerical values.

$$h = 6.6261 * 10^{-27} \frac{\text{cm}^2 * \text{g}}{\text{s}}$$

$$\nu_o = 377107.463 \text{ GHz}$$

$$L = 3 \text{ cm, for collision cell, OR } 7 \text{ cm, for pyrex cell}$$

$$L = (\text{after 2020-01-28}) 3 \text{ cm, for collision cell, OR } 7 \text{ cm, for pyrex cell}$$

$$r_e = 2.8179 * 10^{-13} \text{ cm}$$

$$c = 2.99792458 * 10^{10} \frac{\text{cm}}{\text{s}}$$

$$f_{ge} = 0.34231$$

$$\kappa = \frac{4}{3}$$

$$\mu_B = 9.2740 * 10^{-21} \frac{\text{g cm}^2}{\text{s}^2 \text{ G}}$$

Here is a list of system parameters that are used

α = Angular position of the pass axis of the linear polarizer

β = Starting angular position of the pass axis of the polarimeter QWP

δ = Retardance of the QWP in the polarimeter

And their values

$$\alpha = 20.4^\circ$$

$$\beta = 68.7^\circ$$

$$\delta = 94.54^\circ$$

Bibliography

- [1] H Berry, G Gabrielse, and A E Livingston. Measurement of the stokes parameters of light. Applied Optics, 16:3200–5, 12 1977.
- [2] Nathan Clayburn. Integrated Stokes Parameter Measurements of Spin-Polarized Electron-Impact Excitation of the (3d104s5s)5^3S_1 State of Zinc. PhD thesis, University of Nebraska-Lincoln, 2017.
- [3] Eric Litaker. Studies of rubidium number density and polarization using spectrally-broadened diode lasers. Thesis. <https://unl.box.com/v/litakerThesis>.
- [4] M. Pirbhai, D. M. Ryan, G. Richards, and T. J. Gay. Compact inline optical electron polarimeter. Review of Scientific Instruments, 84(5):053113, May 2013.